YOUR AUTOREGRESSIVE VISUAL MODEL IS A NATIVELY MULTI-TOKEN PREDICTOR : SPECULATIVE COUPLED DECODING FOR FAST AUTOREGRESSIVE VISUAL GENERATION

Junhyuk So[1], **Hyunho Kook**[1], **Chaeyeon Jang**[1], **Eunhyeok Park**[1,2]
POSTECH, South Korea
[1] Department of Computer Science and Engineering
[2] Graduate School of Artificial Intelligence
{junhyukso,kookhh0827,jcy2749,eh.park}@postech.ac.kr

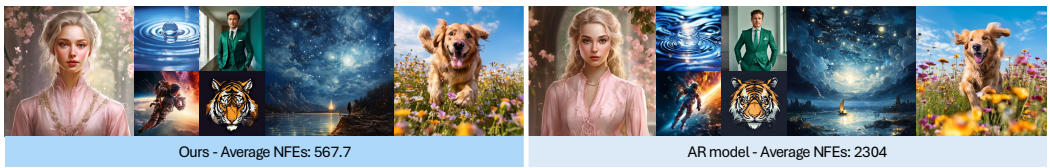

Figure 1: Our **SCD** can be applied to any AR model in a *plug-and-play manner*, maintaining *lossless* performance while providing up to $\sim$ 4x acceleration for image AR and $\sim$ 13x for video AR.

ABSTRACT

Autoregressive (AR) modeling has recently emerged as a promising new paradigm in visual generation, but its practical adoption is severely constrained by the slow inference speed of per-token generation, which often requires thousands of steps to produce a single sample. While several Speculative Decoding (SD)-based methods have been proposed to solve this problem by generating multiple tokens in a single forward step, they suffer from limited speedup, degraded quality, or require the training of a draft model. To solve these problems, we propose a new training-free, lossless SD framework, Speculative Coupled Decoding (SCD), by extending the recently proposed Speculative Jacobi Decoding (SJD). While SJD shows strong potential for accelerating AR generation by combining Jacobi iteration and SD, we found that its acceptance rate is still significantly limited due to the instability arising from the independent sampling process used during draft token generation. To overcome this, we introduce an information-theoretic approach, Coupling, which stabilizes the drafting trajectory of SJD by maximizing the probability of sampling identical draft tokens across consecutive iterations, significantly enhancing the acceptance rate while preserving its lossless property. Remarkably, this method can be applied to any AR model without any training or overhead, yet achieves substantial performance gains, delivering up to a 4.2× speedup in image generation and a 13.6× speedup in video generation compared to standard AR decoding, with zero quality degradation.

1 INTRODUCTION

Recently, autoregressive (AR) modeling has emerged as a cornerstone of modern generative AI, achieving state-of-the-art performance not only in text generation (Touvron et al., 2023) but also across diverse modalities including images (Liu et al., 2024; Sun et al., 2024a), video (Agarwal et al., 2025), 3D meshes (Weng et al., 2025), audio (Du et al., 2024; Wang et al., 2023), and even robotics (Pertsch et al., 2025). Its key strength lies in the ability to unify training and inference across modalities within a single framework, enabling flexible generation, editing, and translation. This cross-domain unification allows models to leverage rich knowledge from different sources, enhancing both understanding and generation (Zhang et al., 2025).

However, the practical power of AR modeling is often constrained by the inherent cost of massive computation and exacerbated memory bottlenecks. Generating a sequence of N tokens requires N AR forward passes, leading to significant latency. The problem becomes particularly severe for high-dimensional data such as images and video, where thousands of tokens are needed to represent a single high-resolution instance, acting as a critical barrier to the real-world deployment of multimodal AR models at scale.

Recently, speculative decoding (SD) (Leviathan et al., 2023) has been actively explored to solve this problem, particularly for large language models (LLMs) in text generation. The core idea is to use computationally smaller draft model to propose multiple candidate tokens fast, which are then verified *in parallel* by the accurate target model. More importantly, SD is a ***lossless*** acceleration method, guaranteeing its output distribution remains theoretically identical to standard AR. However, despite its effectiveness, SD has notable drawbacks: the overhead of training a separate draft model, and limited performance in vision generation tasks (So et al., 2025; Jang et al., 2024).

To address these problems, the Speculative Jacobi Decoding (SJD) (Teng et al., 2024) was proposed, combining Jacobi iteration (Song et al., 2021) with the stochastic verification criterion of SD. SJD uses the output distribution from its own previous verification step as the draft for the next, eliminating the need for a separate, trained draft model, thereby resolving the idle-time bottleneck and demonstrating significant speedups, especially in image generation. However, while SJD shows promise, it delivers only about $\sim 2\times$ speedup in image generation, relatively modest compared to state-of-the-art SD methods in text generation, which achieve over $4\times$ acceleration (Cai et al., 2024).

In this paper, we demonstrate that this problem can be solved with a simple tweak to the SJD process, offering an incredibly high speedup while maintaining the lossless property of SD. Our key finding is that the performance of the SJD is significantly limited by instability in its draft token sampling, leaving substantial room for further improvement. To solve this problem, we propose **speculative Coupled Decoding(SCD)**, a *Coupling* approach between consecutive Jacobi iterations, thereby increasing the probability of sampling identical tokens to promote stability. Since this method does not require any additional training of the original model, we can convert any AR model into an SCD. We demonstrate that our SCD enables a remarkable speedup of 3.8× for AR image generation and 10× for video generation compared to standard AR decoding.

2 Preliminaries

Notation. We denote by X_i^t the token at the i-th position of a sequence X at Jacobi iteration t (defined later). When clear from context, we omit the subscript/superscript i or t to refer to the entire sequence or to the collection of distributions, respectively. Similarly, we denote by $p_i^t(\cdot)$ the token distribution at position i in iteration t. We assume all distributions are on the same support $\mathcal{V}$.

2.1 Speculative Decoding

Speculative Decoding(SD) (Leviathan et al., 2023) is primary technique for accelerating LLMs in the text-generation domain. The main goal of SD is to reduce the number of sequential calls of target model p while ensuring that final outcome matches the original Autoregressive (AR) sampling distribution, $\prod_i p_i(x \mid X_{<i})$. Specifically, we assume two models: a target $p(x)$, which we wish to accelerate, and a draft $q(x)$, which is faster than $p(x)$ but less accurate. SD proceeds as follows:

1. **Drafting**: Sample L draft tokens from the draft distributions, $X_{i:i+L-1} \sim q_{i:i+L-1}(\cdot)$.
2. **Evaluate**:Target model evaluates probabilities along drafted prefixes $\{\, p_j(X_j \mid X_{<j}) \,\}_{j=i}^{i+L}$.
3. **Verify**: Run Alg.3 with (p_i, q_i, X_i) sequentially until a rejection occurs (i.e., the procedure returns $k = 0$); Then *accept* all previously verified tokens.
4. **Repeat**: If the generation is not yet complete, return to **Drafting** and repeat the process.

Transformers natively support the *parallel* evaluation in step (2) via masked attention, ideally in $O(1)$ sequential depth. Thus, if *acceptance* occurs in step (3), this procedure emit multiple tokens in effectively $O(1)$ sequential time, reducing total NFEs compared with standard AR decoding.

Notable advantage of SD is ***lossless*** acceleration. The sampling of Alg. 3 guarantees that even if the input is $X \sim q(\cdot)$, the output Y returned by the algorithm satisfies $Y \sim p(\cdot)$ (Chen et al.,

Algorithm 1 Speculative Jacobi Decoding

Require: AR Model p_θ, Window len. L, Sequence Len N

$p_t^i \leftarrow$ `Random()`
$X_i^t \sim p_i^t \quad \forall i, t$ ◁ Initialize
while $i < N$ **do**
  parallel for $j = i$ to $i + L$: ◁ Drafting
    $X_j^t \sim p_j^t(x)$

  parallel for $j = i$ to $i + L$: ◁ Evaluate
    $p_j^{t+1} \leftarrow p_\theta(\cdot \mid X_{0:j-1}^t)$
  for $j = i$ to $i + L$: ◁ Verify
    $X_j^{t+1}, k \leftarrow \texttt{MRS}(p_j^{t+1}, p_j^t, X_j^t)$
    if $k = 0$: **break;**
  $i \leftarrow j + 1, t \leftarrow t + 1$
end while
return X

Algorithm 2 Pseudo Code for our **SCD**

Require: AR Model p_θ, Window len. L, Sequence Len N

$p_t^i \leftarrow$ `Random()`
$X_i^t \sim p_i^t \quad \forall i, t$ ◁ Initialize
while $i < N$ **do**
  parallel for $j = i$ to $i + L$: ◁ Drafting
    $X_j^t, _ \leftarrow \texttt{MRS}(p_j^t, p_j^{t-1}, X_j^t)$ **Maximal**
    $X_j^t, _ \leftarrow \texttt{GS}(p_j^t, p_j^{t-1}, G_j)$ **Gumbel**
  parallel for $j = i$ to $i + L$: ◁ Evaluate
    $p_j^{t+1} \leftarrow p_\theta(\cdot \mid X_{0:j-1}^t)$
  for $j = i$ to $i + L$: ◁ Verify
    $X_j^{t+1}, k \leftarrow \texttt{MRS}(p_j^{t+1}, p_j^t, X_j^t)$
    if $k = 0$: **break;**
  $i \leftarrow j + 1, t \leftarrow t + 1$
end while
return X

2023). Because each Markov chain follows valid sampling from p until the first rejection occurs, the theoretical correctness of speculative decoding is ensured. As shown in Alg. 3, the acceptance probability per token, $\min\{1, p(x)/q(x)\}$, is the key factor that determines the overall speedup. We formalize it in following proposition:

Proposition 1 *Let q be the draft distribution and $x \sim q(x)$, then, final output from* `MRS`*(Alg.3) strictly follow the distribution of target model $p(x)$. Moreover, the acceptance rate of this algorithm is defined as*

$$\mathbb{E}_{x\sim q(x_i)} min(1, \frac{p(x)}{q(x)}) = 1 - \mathcal{D}_{TV}(p, q)$$

where $\mathcal{D}_{TV}$ denotes total variation $\frac{1}{2}\sum_v |p(v) - q(v)|$.

Proof: See appendix. Typically, standard SD methods employ a "cheaper" AR model to produce draft tokens/distributions. While this strategy has shown promising results in the text-generation domain (Cai et al., 2024), it has several drawbacks: the need to train a separate draft model, communication bottlenecks between the draft and target models, and limited speedups in non-text AR generation domains (So et al., 2025; Jang et al., 2024). These issues have hindered the adoption of SD techniques beyond text, limiting the potential of AR modeling across different modalities.

Algorithm 3 `MRS`(p,q,x); Rejection Sampling

Input: Distribution P, Q. Tokens $X \sim Q$
Output: Random variable Y, Accept signal k

if $u \sim \mathcal{U}[0, 1] \leq \min(1, \frac{P(X)}{Q(X)})$
  return $Y = X, 1$
$R \leftarrow \text{norm}(\max(0, P(x) - Q(x)))$
return $Y \sim R, 0$

Algorithm 4 `GS`(P, Q, G); Gumbel Sharing

Input: Distributions P, Q Gumbel Noise G.
Output: Coupled pair (X, Y).

$(g_1, \ldots, g_{|\mathcal{V}|}) \leftarrow G$
$X \leftarrow \text{argmax}_{i\in\mathcal{V}}(\log(P_i) + g_i)$
$Y \leftarrow \text{argmax}_{i\in\mathcal{V}}(\log(Q_i) + g_i)$
return (X, Y)

2.2 Speculative Jacobi Decoding

Speculative Jacobi Decoding (SJD) Teng et al. (2024) is a pioneering, training-free algorithm to solve the aforementioned problems of standard speculative decoding. As depicted in Algorithm 1, SJD eliminates the need for a separate draft model $q(\cdot)$. Instead, it leverages the probability distribution from its own previous validation step as the draft for the next iteration. This "Self-SD" approach does not impact the theoretical accuracy guarantees of speculative decoding, because the verification mechanism (Alg. 3) ensures the output is always a valid sample from the target model's

distribution, regardless of the input draft. This framework makes the process highly efficient as it removes the overhead of training a separate model and eliminates the idle time where the target model would wait for draft tokens. Due to these properties, SJD first achieves a ∼2x speedup in AR image generation domain, while retaining its lossless and training-free nature.

3 Motivation and Analysis

Despite achieving a ∼2x speedup in image AR, we find that performance potential of SJD is *significantly limited* by the variance introduced during its stochastic draft sampling process. To gain an intuitive understanding of this, we start with an analysis of the acceptance rate of SJD. At iteration t in SJD, the target distribution is $p^t(\cdot)$ and the draft distribution is $p^{t-1}(\cdot)$. As noted in Proposition 1, the acceptance rate can be expressed in terms of the Total Variation, as follows :

$$\beta_i^{(t)} = 1 - \mathcal{D}_{TV}\left(p_i^{(t)}(x), p_i^{(t-1)}(x)\right) \tag{1}$$

$$= 1 - \mathcal{D}_{TV}\left(p_\theta\left(\cdot \,\middle|\, X_{<i}^{(t-1)}\right), p_\theta\left(\cdot \,\middle|\, X_{<i}^{(t-2)}\right)\right), \tag{2}$$

where p_θ denotes the autoregressive model and $X_{<i}$ denotes the prefixes $\{X_{i-1}, X_{i-2}, \dots\}$. As shown in Eq. 2, The acceptance rate $\beta_i^{(t)}$ is directly influenced by the *context change* between iterations $t-1$ and $t-2$. In other words, the acceptance rate for token i is driven by changes in its *prefixes*, including both previously accepted tokens but also the other rejected tokens in the draft. This leads directly to the following observation:

Observation 1 *High context similarity between consecutive drafts tends to yield a higher speedup.*

This can be easily validated by Eq. 2: the greater the similarity between the contexts $X_{<i}^{(t-1)}$ and $X_{<i}^{(t-2)}$, the more similar their corresponding output distributions $p_\theta(\cdot|X_{<i})$ will be (under a mild Lipschitzness assumption on the model's logits from tokens). This results in a lower TV distance and, consequently, a higher acceptance rate β.

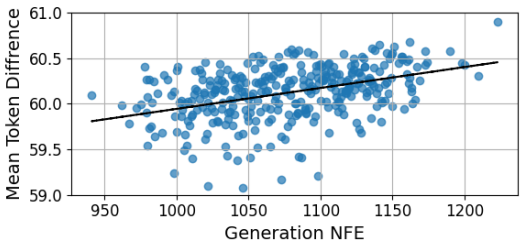

Figure 2: Generation NFE v.s Mean Token Difference during SJD with window size $L = 64$. As shown, a sample that is generated with smaller NFE tends to have small mean token difference.

We also empirically validate it in Fig. 2, plotting the 300 independent samples with their mean number of changed tokens between consecutive sequence drafts (Hamming distance) against the total number of function evaluations (NFE) required for SJD generation. As shown, there is a strong correlation between these two metrics, indicating that context similarity plays a crucial role for faster generation in SJD.

However, despite this correlation, Fig. 2 shows that the average number of token difference is approximately 94% tokens - 60 of window size 64 -, indicating significantly large portion of tokens are changed in each iteration. We observe that this high degree of change not only critically limits SJD's single iteration acceptance rate but also poses a more severe problem if we consider behavior on multiple consecutive iterations, the *convergence* of SJD.

Observation 2 *The per-token acceptance rate β_i^t during the SJD process exhibits high variance and does not show converging behavior.*

Ideally, the acceptance rate for a given token should increase over the SJD iterations. As the left-most context becomes filled with stable, accepted tokens, an "improvement signal" should propagate to the right, progressively enhancing the quality of the draft sequences. However, our empirical results reveal the opposite behavior. Fig. 3(a) plots the trajectory of β_i^t for representative tokens, showing that the acceptance rate frequently fluctuates without any consistent upward trend. This instability is further confirmed in Fig. 3(c) (blue line), which aggregates the statistics across all tokens. After an initial jump, the mean acceptance rate not only remains low but also fails to improve, exhibiting random fluctuations with high variance throughout the process.

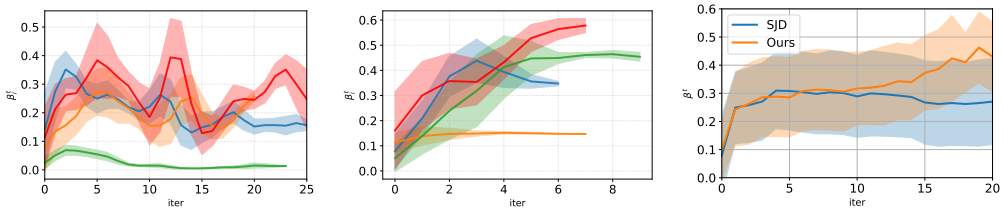

(a) **SJD** β_i^t convergence (b) **Ours** β_i^t convergence (c) β_i^t statistics (Mean - Var)

Figure 3: (a), (b) The trajectory of tokenwise acceptance rate β_i^t during the jacobi iterations (a) Standard SJD shows most tokens have large variation during iteration and do not exhibit improvement behavior. (b) After applying our coupled sampler π_{MC}. Now most of tokens has very small fluctuation, showing general upward trends. (c) Mean and variance of β_i^t across all token index. While standard SJD does not show improvement, ours shows clear upward, refining behavior.

3.1 Analysis

We then investigate the root cause of this low context similarity. Since the context sequences $X^{(t)}$ are realizations of random variables drawn from $p^{(t)}(\cdot)$, a natural way to quantify their similarity is by measuring the **collision probability**, defined as $\Pr[X_i^{(t)} = X_i^{(t-1)}]$. As described in Algorithm 1, the drafting stage of SJD (Line 5) samples the draft token $X_i^{(t)}$ *independently* from its distribution $p_i^t(x)$. Their collision probability between $X_i^{(t)}$ and $X_i^{(t-1)}$ can be analytically computed as :

Proposition 2 (SJD Collision Probability) *Standard SJD has the following collision probability for token i at iteration t:*

$$C_{SJD}(p^{(t)}, p^{(t-1)}) = \sum_{x \in \mathcal{V}} p_i^{(t)}(x) \cdot p_i^{(t-1)}(x)$$

where $\mathcal{V}$ denotes the vocabulary. This value is bounded as follows:

$$C_{SJD}(p, q) \leq e^{-1/2 \cdot (H_2(p) + H_2(q))}$$

where $H_2(p) = -log(\sum_x p(x)^2)$ is the Rényi-2 entropy of p.

Proof: See appendix. As shown, even when two distributions are similar, their collision probability is constrained by the (Rényi-2) entropy of the underlying distributions and vocabulary sizes. Unfortunately, unlike text AR models, visual AR models are known to generate very flat distributions (So et al., 2025). This is because of the inherent redundancy in visual tokens and the complexity of visual patterns makes a large number of different tokens plausible continuations of a sequence.

We also visualize the empirical collision probability, C_{SJD}, during the SJD process. The Fig. 4 (a) shows most of its values remain at an extremely low value, and (c) illustrates that this value is nearly zero regardless of whether the TV distance is small. Consequently, the standard SJD propagates different contextual information to subsequent tokens in each iteration, significantly destabilizing iteration and causing the convergence to fluctuate unpredictably. We identify this discrepancy between the proximity in probability space and realized token space as *key factor* limiting the speedup.

4 Methods

Our main idea is that making ***Coupling*** ((Lindvall, 2002)) between the draft distributions from consecutive iterations can increase the collision probability without compromising the theoretical lossless correctness of the SJD. To formalize, we begin with mathematical definition of coupling :

Definition 1 (Coupling) *For two distributions $P(\cdot)$ and $Q(\cdot)$ on the same support $\mathcal{V}$, a joint distribution $\pi(\cdot, \cdot)$ over $\mathcal{V} \times \mathcal{V}$ is a **Coupling** of P and Q if its marginals satisfy:*

$$\sum_{y \in \mathcal{V}} \pi(x, y) = P(x) \quad \textit{and} \quad \sum_{x \in \mathcal{V}} \pi(x, y) = Q(y)$$

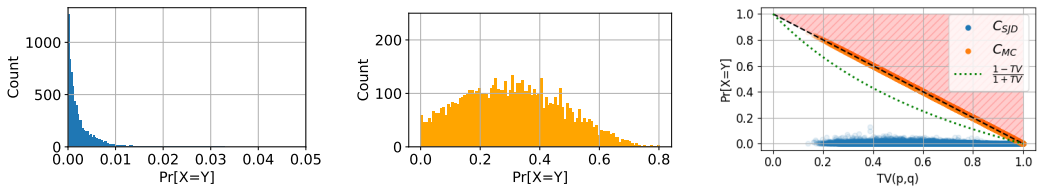

(a) **SJD** $\Pr[X = Y]$ histogram (b) **Ours** $\Pr[X = Y]$ histogram (c) $\mathcal{D}_{TV}$ v.s $\Pr[X = Y]$

Figure 4: Visualization of Collision probabilities. (a) During standard SJD, C_{SJD} are concentrated on extremely small values. (b) Our Coupler elevates this to much higher values, significantly enhancing the context similarity. (c) Standard SJD has a low $\Pr[X = Y]$ even when the corresponding TV distance is low. The green dot-line denotes the π_{GS} lower bound $\pi_{GS} \geq (1-\mathcal{D}_{TV})/(1+\mathcal{D}_{TV})$.

The key insight lies in the marginalization property of a coupling. If we sample a pair of variables from a joint distribution $\pi(x, y)$, the marginal distribution of each individual variable remains identical to its original distribution (e.g., $P(x)$ and $Q(y)$). Therefore, using a token sampled from a coupling is a provably valid replacement for independent sampling within the SJD framework. We formally stated this in the following theorem:

Theorem 1 *Let $\Pi_i^{(t)}$ be the set of all possible couplings between $p_i^{(t)}$ and $p_i^{(t-1)}$. If we sample a pair $(X_i^{(t)}, X_i^{(t-1)}) \sim \pi(\cdot, \cdot)$ for any $\pi \in \Pi_i^{(t)}$ and use $X_i^{(t)}$ as the draft token in Algorithm 1, the final output distribution still correctly matches the target model's distribution.*

For any given coupling π, we can define its effectiveness using a metric called the **Coupling Cost**, denoted $C(\pi)$. This cost measures the probability of sampling identical variables from the joint distribution, which is the same metric we previously referred to as the collision probability:

Definition 2 (Coupling Cost) *Let $\pi_{P,Q}$ be a coupling of distributions P and Q as per Definition 1. The Coupling Cost is defined as:*

$$C(\pi_{P,Q}) = \Pr_{(X,Y)\sim\pi_{P,Q}}[X = Y] = \mathbb{E}_{(X,Y)\sim\pi_{P,Q}} \mathbb{1}\{X = Y\}$$

Finally, our main objective can be safely reframed as finding an alternative coupling, π^*, that **maximizes** this cost, thereby promoting context similarity without compromising the exactness guarantee of the framework. We next present alternative couplings that achieve this objective.

4.1 Maximal Coupling

Consider the computation graph of X^t and $p^t(x)$ during the SJD process :

$$X^{t-2} \to p^{t-1}(X) \to X^{t-1} \to p^t(X) \to X^t \tag{3}$$

As shown, at the time of sampling step for $X^{(t)}$, we have access to the full information of two probability distributions $p^{(t)}$ and $p^{(t-1)}$. As is well-established in many literature on information theory and optimal transport (Villani et al., 2008; Bavarian et al., 2016), *having complete information of both distributions allows us for the construction of a **maximal coupling***, which has the cost of $c(\pi_{p,q}) = 1 - \mathcal{D}_{TV}(p, q)$ that any two distribution can maximally have.

In Algorithm 2, we present the implementation of SJD with draft sampling with maximal coupling process. As shown, the only modification required is in the drafting phase (Line 4), where we now sample the draft token X^t using a *coupled sampler* instead of sampling it independently from $p_i^t(\cdot)$. Interestingly, as shown, the implementation of this coupling is exactly identical with the modified rejection sampling, $\texttt{MRS}(\cdot)$ (Alg.3) which we used for speculative decoding verification process. This can be easily validated by the fact that $\texttt{MRS}(\cdot)$ returns $Y \sim P$ from an input $X \sim Q$, ensuring that the marginals of the generated pair (Y, X) match P and Q, which satisfies the definition of a coupling. Moreover, as established in Proposition 1, the acceptance rate $\texttt{MRS}(\cdot)$ - probability of $\Pr[X = Y]$ - is $1-\mathcal{D}_{TV}(p, q)$. This value is the theoretical upper bound of coupling cost, confirming that this procedure constitutes a maximal coupling. We formally state this as follows:

Table 1: Evaluation results of AR Image generation model, Lumina-mGPT, on MS-COCO dataset.

Configuration		NFE (↓)	Latency (↓) (A100)	Acceleration (↑) NFE	Acceleration (↑) Latency	FID (↓)	IS (↑)	CLIP-Score (↑)
A	*Vanilla AR*	2390	102.03s	1.00×	1.00×	30.79	32.81	31.31
B	SJD (L=16)	1058.6	43.02s	2.25×	2.37x	30.77	32.78	31.32
D	+ **Ours** (π_{MC})	**814.5**	**32.75s**	**2.94×**	**3.12x**	30.73	33.56	31.32
D	+ **Ours** (π_{GS})	819.4	32.89s	2.92×	3.10x	30.78	32.77	31.37
B	SJD (L=32)	1031.2	42.99s	2.32×	2.37x	30.78	32.82	31.31
D	+ **Ours** (π_{MC})	666.0	26.77s	3.59×	3.81x	30.79	33.56	31.32
D	+ **Ours** (π_{GS})	**652.3**	**26.44s**	**3.66×**	**3.86x**	30.75	32.91	31.39
B	SJD (L=64)	1035.9	42.98s	2.31×	2.37x	30.81	32.76	31.31
D	+ **Ours** (π_{MC})	**567.7**	24.41s	**4.21×**	4.18x	30.83	33.43	31.37
D	+ **Ours** (π_{GS})	568.0	**24.24s**	4.21x	**4.21x**	30.90	32.80	31.37
C	GSD (L=32,G=3)	925.9	38.98s	2.58×	2.62x	31.50	29.76	31.33
C	GSD (L=32,G=10)	701.4	29.13s	3.40×	3.50x	33.21	26.78	31.25

Theorem 2 *Let the pair (X,Y) be generated by Algorithm 3. Then, their resulting joint distribution* $(X, Y) \sim \pi_{MC}$*, is a valid coupling of P and Q. Moreover, its coupling cost,*

$$C(\pi_{MC}) = 1 - \mathcal{D}_{TV}(P, Q)$$

is the upper bound for the cost of any $\pi \in \Pi$ *with* P *and* Q*.*

As illustrated in Fig. 4 (c), this upper bound, represented by the black dashed line, shows a significant gap compared to the coupling cost of standard SJD (C_{SJD}). Applying maximal coupling within SJD, elevates this low values to their upper bound (orange dots), thereby strongly promoting high context similarity and achieving a greater speedup. We also show the distribution of $C(\pi_{MC})$ in Fig. 4 (b). In Fig. 3 (b), (c), we show the trajectories and statistics of the β^t, during iterations with MC-SJD. As shown, most tokens now exhibit minimal fluctuation with a general upward trend, resulting in a much higher overall acceptance rate compared to standard SJD, leading to lower NFEs.

4.2 Gumbel Coupling

In Alg. 4, we also propose *Gumbel Coupling* (π_{GS}), which have similar coupling cost with π_{MC} but have different characteristic and convergence behavior. As shown, this algorithm is based on the Gumbel-Max trick that relies on sharing the same random noise vector to couple two categorical sampling processes. `GS` versioned SCD can also be seen in Alg. 2. We establish its validity and provide a lower bound for its cost:

Theorem 3 *Let the pair (X,Y) be generated by Alg. 4. Then, their resulting joint distribution* $(X, Y) \sim \pi_{GS}$*, is a valid coupling of P and Q. Its worst-case coupling cost is lower-bounded by:*

$$C(\pi_{GS}) \geq (1 - \mathcal{D}_{TV}(P, Q))/(1 + \mathcal{D}_{TV}(P, Q))$$

As shown in Fig. 4 (c), this lower bound is significantly greater than the independence coupling π_{SJD} and almost tight to the maximal $1 - \mathcal{D}_{TV}$ line, thus achieving performance comparable to π_{MC}. Moreover, π_{GS} can even yield better NFEs in some tasks. Since this lower bound is applicable to any pair of distributions during an iteration, this Gumbel Coupling promotes more *long-range stabilization*, whereas π_{MC} can be seen as greedy optimization within each consecutive iteration. We found that this behavior can be beneficial in tasks where draft prediction is relatively easy, so that keeping early draft tokens unchanged can have more beneficial effect than continually updating them with slightly more accurate information.

Table 2: Video generation results on Cosmos1-AR-4B, on real-state-10k dataset.

Metric	Vanilla	L=16			L=32			L=64			L=128		
	AR	SJD	+ π_{MC}	+ π_{GS}	SJD	+ π_{MC}	+ π_{GS}	SJD	+ π_{MC}	+ π_{GS}	SJD	+ π_{MC}	+ π_{GS}
NFE (↓)	7680	2272.8	1990.5	**1940.6**	1886.4	1293.7	**1267.3**	1802.3	835.9	**810.7**	1789.9	577.8	**564.4**
Latency (s) (↓)	157.25	54.12	48.93	**47.97**	48.43	32.36	**32.01**	48.19	22.38	**21.58**	47.73	15.87	**13.60**
FVD (↓)	156.9	157.1	159.3	154.8	153.2	155.8	153.6	163.6	155.8	152.9	158.3	157.8	152.4

5 Experimental Results

In experiments section, we mainly focus on validating two aspects : (i) How much acceleration can we gain by applying our method atop SJD, (ii) Does our algorithm truly preserve generation quality, although we show it theoretically.

Setup Similar to original SJD paper, we mainly evaluate with Lumina-mGPT (Liu et al., 2024) for AR image generation. We also evaluate our method with the more SOTA AR Image model, Janus-Pro (Chen et al., 2025) and Lumina-mGPT-2 (Xin et al., 2025), to validate our method's generalization. Moreover, beyond image generation, we also evaluate with an AR video generation model, Cosmos-1-AR (Agarwal et al., 2025), which has significantly longer generation length.

Metrics and Datasets To evaluate the quality, we measured FID (Heusel et al., 2017) , which measures the distribution distance compared to reference and generated datasets, with IS (Barratt & Sharma, 2018) and CLIP score (Radford et al., 2021). To evaluate the speed, we measure the number of function evaluations (NFEs), which indicates the number of sequential forward steps for generation, and the real latency on 1x NVIDIA A100 device. We mainly use MS-COCO (Lin et al., 2014) and Parti-prompt (Yu et al., 2022) dataset for image generation and Real-Estate-10k for video generation. More details are in appendix.

Baselines We benchmarked our method against three baselines: (A) Autoregressive decoding (*Vanilla AR*), (B) Speculative Jacobi Decoding (SJD) (Teng et al., 2024) (C) Grouped Speculative Decoding (GSD) (So et al., 2025), which is recently proposed training-free lossy SD methods for image generation and (D) Ours. We mainly compare our method against these baselines because they are training-free SD, thus enabling a fair comparison, and they demonstrate most superior performance. We also provide comparisons with training-based SD models in Appendix.

Results Table 1 presents our main results for AR image generation on Lumina-mGPT. As shown, our method (D) accelerates the *Vanilla AR* (A) by up to 4.2x and SJD (B) by 1.8x without compromising exactness guarantee, maintaining identical FID, IS and CLIP scores. Notably, while standard SJD fails to achieve meaningful speedup with an increased window size (L), our SCD shows higher acceleration as the window size grows, strongly suggesting that our coupling helps to stabilize SJD's convergence. Finally, (C) , lossy-SD method GSD, also significantly reduces the NFE, but results in a degradation of the FID and CLIP scores. Our method, in contrast, shows an even faster speedup than lossy GSD while maintaining quality exactness. In Table 3, we report results of Janus-Pro (7B). As shown, our method consistently accelerates the standard SJD process by up to 2.1x, achieving a final step compression of 3.7x. We also present results on Parti-prompt dataset and Lumina-mGPT-2 in Tab. 5, 6 and Fig. 9. As shown, our SCD still shows up to $4.4\times$ speedup compared to AR in various datasets and models.

Table 3: Janus-Pro (7B) on MS-COCO 2017.

Config		NFE (↓)	Latency(s)(↓)	FID (↓)	IS (↑)
A	*Vanilla AR*	576	13.218	37.96	22.39
B	SJD ($L = 16$)	319.93	10.213	37.96	22.25
D	+ **Ours**(π_{MC})	**190.21**	6.345	37.46	22.19
D	+ **Ours**(π_{GS})	**189.99**	6.336	37.13	22.53
B	SJD ($L = 32$)	318.01	10.582	37.76	21.80
D	+ **Ours**(π_{MC})	**154.76**	5.471	38.34	22.17
D	+ **Ours**(π_{GS})	**154.42**	5.388	37.49	22.43

In Table 2, We depict the results on AR video generation model, Cosmos-1-AR. Notably, our method achieves up to 13.6x actual acceleration with no loss in quality, outperforming other methods in significant margin. We believe this large acceleration mainly stems from the strong temporal redundancy between consecutive frames in video AR; thus making draft prediction relatively easy and thereby enabling the full utilization of longer draft window lengths.

Qualitative Results: We also performed a qualitative comparison experiment to visualize that our method does not degrade generation quality. As shown in Fig. 1, our method yields outputs that are visually indistinguishable from the AR model while achieving the $\sim$4.2$\times$ acceleration. We provide more visualizations in the Appendix Fig. 7, 8, 9, 10.

6 CONCLUSION

In this paper, we identify and resolve a critical performance bottleneck in the recently proposed Speculative Jacobi Decoding (SJD). Specifically, we find that its acceptance rate is significantly limited by draft context instabilities, arising from its independent sampling process. To solve this, we propose Speculative Coupled Decoding (SCD), which use *Coupling* to replace independent sampling and stabilize the Jacobi iteration trajectory by increasing the probability of sampling identical tokens, transferring distributional similarity to the realized token space. As a result, we show that this simple tweak can remarkably enhance the speedup in visual AR, achieving up to 4.2× in image and 13.6× in video, all without any quality degradation and additional training.

REFERENCES

Niket Agarwal, Arslan Ali, Maciej Bala, Yogesh Balaji, Erik Barker, Tiffany Cai, Prithvijit Chattopadhyay, Yongxin Chen, Yin Cui, Yifan Ding, et al. Cosmos world foundation model platform for physical ai. *arXiv preprint arXiv:2501.03575*, 2025.

Gregor Bachmann, Sotiris Anagnostidis, Albert Pumarola, Markos Georgopoulos, Artsiom Sanakoyeu, Yuming Du, Edgar Schönfeld, Ali Thabet, and Jonas Kohler. Judge decoding: Faster speculative sampling requires going beyond model alignment. *arXiv preprint arXiv:2501.19309*, 2025.

Jinze Bai, Shuai Bai, Yunfei Chu, Zeyu Cui, Kai Dang, Xiaodong Deng, Yang Fan, Wenbin Ge, Yu Han, Fei Huang, et al. Qwen technical report. *arXiv preprint arXiv:2309.16609*, 2023.

Shane Barratt and Rishi Sharma. A note on the inception score. *arXiv preprint arXiv:1801.01973*, 2018.

Mohammad Bavarian, Badih Ghazi, Elad Haramaty, Pritish Kamath, Ronald L Rivest, and Madhu Sudan. Optimality of correlated sampling strategies. *arXiv preprint arXiv:1612.01041*, 2016.

Vasile Berinde. Approximating fixed points of weak contractions using the picard iteration. In *Nonlinear Analysis Forum*, volume 9, pp. 43–54, 2004.

Oscar Brown, Zhengjie Wang, Andrea Do, Nikhil Mathew, and Cheng Yu. Dynamic depth decoding: Faster speculative decoding for llms. *arXiv preprint arXiv:2409.00142*, 2024.

Tom Brown, Benjamin Mann, Nick Ryder, Melanie Subbiah, Jared D Kaplan, Prafulla Dhariwal, Arvind Neelakantan, Pranav Shyam, Girish Sastry, Amanda Askell, et al. Language models are few-shot learners. *Advances in neural information processing systems*, 33:1877–1901, 2020.

Tianle Cai, Yuhong Li, Zhengyang Geng, Hongwu Peng, Jason D Lee, Deming Chen, and Tri Dao. Medusa: Simple llm inference acceleration framework with multiple decoding heads. *arXiv preprint arXiv:2401.10774*, 2024.

Charlie Chen, Sebastian Borgeaud, Geoffrey Irving, Jean-Baptiste Lespiau, Laurent Sifre, and John Jumper. Accelerating large language model decoding with speculative sampling. *arXiv preprint arXiv:2302.01318*, 2023.

Xiaokang Chen, Zhiyu Wu, Xingchao Liu, Zizheng Pan, Wen Liu, Zhenda Xie, Xingkai Yu, and Chong Ruan. Janus-pro: Unified multimodal understanding and generation with data and model scaling. *arXiv preprint arXiv:2501.17811*, 2025.

Chaorui Deng, Deyao Zhu, Kunchang Li, Chenhui Gou, Feng Li, Zeyu Wang, Shu Zhong, Weihao Yu, Xiaonan Nie, Ziang Song, et al. Emerging properties in unified multimodal pretraining. *arXiv preprint arXiv:2505.14683*, 2025.

Zhihao Du, Yuxuan Wang, Qian Chen, Xian Shi, Xiang Lv, Tianyu Zhao, Zhifu Gao, Yexin Yang, Changfeng Gao, Hui Wang, et al. Cosyvoice 2: Scalable streaming speech synthesis with large language models. *arXiv preprint arXiv:2412.10117*, 2024.

Martin Heusel, Hubert Ramsauer, Thomas Unterthiner, Bernhard Nessler, and Sepp Hochreiter. Gans trained by a two time-scale update rule converge to a local nash equilibrium. *Advances in neural information processing systems*, 30, 2017.

Aaron Hurst, Adam Lerer, Adam P Goucher, Adam Perelman, Aditya Ramesh, Aidan Clark, AJ Ostrow, Akila Welihinda, Alan Hayes, Alec Radford, et al. Gpt-4o system card. *arXiv preprint arXiv:2410.21276*, 2024.

Doohyuk Jang, Sihwan Park, June Yong Yang, Yeonsung Jung, Jihun Yun, Souvik Kundu, Sung-Yub Kim, and Eunho Yang. Lantern: Accelerating visual autoregressive models with relaxed speculative decoding. *arXiv preprint arXiv:2410.03355*, 2024.

Yaniv Leviathan, Matan Kalman, and Yossi Matias. Fast inference from transformers via speculative decoding. pp. 19274–19286, 2023.

Tsung-Yi Lin, Michael Maire, Serge Belongie, James Hays, Pietro Perona, Deva Ramanan, Piotr Dollár, and C Lawrence Zitnick. Microsoft coco: Common objects in context. In *Computer vision–ECCV 2014: 13th European conference, zurich, Switzerland, September 6-12, 2014, proceedings, part v 13*, pp. 740–755. Springer, 2014.

Torgny Lindvall. *Lectures on the coupling method*. Courier Corporation, 2002.

Dongyang Liu, Shitian Zhao, Le Zhuo, Weifeng Lin, Yu Qiao, Hongsheng Li, and Peng Gao. Lumina-mgpt: Illuminate flexible photorealistic text-to-image generation with multimodal generative pretraining. *arXiv preprint arXiv:2408.02657*, 2024.

Adam Paszke, Sam Gross, Francisco Massa, Adam Lerer, James Bradbury, Gregory Chanan, Trevor Killeen, Zeming Lin, Natalia Gimelshein, Luca Antiga, et al. Pytorch: An imperative style, high-performance deep learning library. *Advances in neural information processing systems*, 32, 2019.

Karl Pertsch, Kyle Stachowicz, Brian Ichter, Danny Driess, Suraj Nair, Quan Vuong, Oier Mees, Chelsea Finn, and Sergey Levine. Fast: Efficient action tokenization for vision-language-action models. *arXiv preprint arXiv:2501.09747*, 2025.

Alec Radford, Jong Wook Kim, Chris Hallacy, Aditya Ramesh, Gabriel Goh, Sandhini Agarwal, Girish Sastry, Amanda Askell, Pamela Mishkin, Jack Clark, et al. Learning transferable visual models from natural language supervision. In *International conference on machine learning*, pp. 8748–8763. PmLR, 2021.

Andy Shih, Suneel Belkhale, Stefano Ermon, Dorsa Sadigh, and Nima Anari. Parallel sampling of diffusion models. *Advances in Neural Information Processing Systems*, 36:4263–4276, 2023.

Junhyuk So, Juncheol Shin, Hyunho Kook, and Eunhyeok Park. Grouped speculative decoding for autoregressive image generation. *arXiv preprint arXiv:2508.07747*, 2025.

Yang Song, Chenlin Meng, Renjie Liao, and Stefano Ermon. Accelerating feedforward computation via parallel nonlinear equation solving. In *International Conference on Machine Learning*, pp. 9791–9800. PMLR, 2021.

Peize Sun, Yi Jiang, Shoufa Chen, Shilong Zhang, Bingyue Peng, Ping Luo, and Zehuan Yuan. Autoregressive model beats diffusion: Llama for scalable image generation. *arXiv preprint arXiv:2406.06525*, 2024a.

Ziteng Sun, Ananda Theertha Suresh, Jae Hun Ro, Ahmad Beirami, Himanshu Jain, and Felix Yu. Spectr: Fast speculative decoding via optimal transport. *Advances in Neural Information Processing Systems*, 36:30222–30242, 2023.

Ziteng Sun, Uri Mendlovic, Yaniv Leviathan, Asaf Aharoni, Jae Hun Ro, Ahmad Beirami, and Ananda Theertha Suresh. Block verification accelerates speculative decoding. *arXiv preprint arXiv:2403.10444*, 2024b.

Chameleon Team. Chameleon: Mixed-modal early-fusion foundation models. *arXiv preprint arXiv:2405.09818*, 2024.

Yao Teng, Han Shi, Xian Liu, Xuefei Ning, Guohao Dai, Yu Wang, Zhenguo Li, and Xihui Liu. Accelerating auto-regressive text-to-image generation with training-free speculative jacobi decoding. *arXiv preprint arXiv:2410.01699*, 2024.

Hugo Touvron, Thibaut Lavril, Gautier Izacard, Xavier Martinet, Marie-Anne Lachaux, Timothée Lacroix, Baptiste Rozière, Naman Goyal, Eric Hambro, Faisal Azhar, et al. Llama: Open and efficient foundation language models. *arXiv preprint arXiv:2302.13971*, 2023.

Aaron Van Den Oord, Oriol Vinyals, et al. Neural discrete representation learning. *Advances in neural information processing systems*, 30, 2017.

Cédric Villani et al. *Optimal transport: old and new*, volume 338. Springer, 2008.

Chengyi Wang, Sanyuan Chen, Yu Wu, Ziqiang Zhang, Long Zhou, Shujie Liu, Zhuo Chen, Yanqing Liu, Huaming Wang, Jinyu Li, et al. Neural codec language models are zero-shot text to speech synthesizers. *arXiv preprint arXiv:2301.02111*, 2023.

Haohan Weng, Zibo Zhao, Biwen Lei, Xianghui Yang, Jian Liu, Zeqiang Lai, Zhuo Chen, Yuhong Liu, Jie Jiang, Chunchao Guo, et al. Scaling mesh generation via compressive tokenization. In *Proceedings of the Computer Vision and Pattern Recognition Conference*, pp. 11093–11103, 2025.

Yi Xin, Juncheng Yan, Qi Qin, Zhen Li, Dongyang Liu, Shicheng Li, Victor Shea-Jay Huang, Yupeng Zhou, Renrui Zhang, Le Zhuo, et al. Lumina-mgpt 2.0: Stand-alone autoregressive image modeling. *arXiv preprint arXiv:2507.17801*, 2025.

Jiahui Yu, Yuanzhong Xu, Jing Yu Koh, Thang Luong, Gunjan Baid, Zirui Wang, Vijay Vasudevan, Alexander Ku, Yinfei Yang, Burcu Karagol Ayan, et al. Scaling autoregressive models for content-rich text-to-image generation. *arXiv preprint arXiv:2206.10789*, 2(3):5, 2022.

Xinjie Zhang, Jintao Guo, Shanshan Zhao, Minghao Fu, Lunhao Duan, Jiakui Hu, Yong Xien Chng, Guo-Hua Wang, Qing-Guo Chen, Zhao Xu, et al. Unified multimodal understanding and generation models: Advances, challenges, and opportunities. *arXiv preprint arXiv:2505.02567*, 2025.

Qingqing Zhao, Yao Lu, Moo Jin Kim, Zipeng Fu, Zhuoyang Zhang, Yecheng Wu, Zhaoshuo Li, Qianli Ma, Song Han, Chelsea Finn, et al. Cot-vla: Visual chain-of-thought reasoning for vision-language-action models. In *Proceedings of the Computer Vision and Pattern Recognition Conference*, pp. 1702–1713, 2025.

Tinghui Zhou, Richard Tucker, John Flynn, Graham Fyffe, and Noah Snavely. Stereo magnification: Learning view synthesis using multiplane images. *ACM Trans. Graph. (Proc. SIGGRAPH)*, 37, 2018. URL https://arxiv.org/abs/1805.09817.

APPENDIX

A IMPLEMENTATION DETAILS

Algorithm 5 Speculative Coupled Decoding (π_{MC})

Require: AR Model p_θ, draft Length L, Max Sequence N

$p_t^i \leftarrow$ `Random()`
$X_i^t \sim p_i^t \quad \forall i, t$ ◁ Initialize
while $i < N$ **do**
  parallel for $j = i$ to $i + L$: ◁ Evaluate
    $p_j^{t+1} \leftarrow p_\theta(\cdot \mid X_{0:j-1}^t)$
  $Accept \leftarrow i + L$
  parallel for $j = i$ to $i + L$: ◁ Verify & Drafting with Vectorized `MRS`
    $k, X_j^{t+1} \leftarrow$ `MRS`$(p_j^{t+1}, p_j^t, X_j^t)$
    if $k = 0$ **and** $Accept = i + L$: ◁ Find first rejection index
      $Accept \leftarrow j$
  $i \leftarrow Accept + 1$, $t \leftarrow t + 1$
end while
return X

Algorithm 6 Speculative Coupled Decoding (π_{GS})

Require: AR Model p_θ, draft Length L, Max Sequence N

$p_t^i \leftarrow$ `Random()` ◁ Initialize state
$X_i^t \sim p_i^t \quad \forall i, t$ ◁ //Initialize
while $i < N$ **do**
  parallel for $j = i$ to $i + L$: ◁ Drafting
    $G_j \leftarrow$ `SampleGumbelNoiseUsingHash`(j) ◁ G_j.shape = $[\mathcal{V}]$
    $X_j \leftarrow \text{argmax}_{i \in \mathcal{V}}(\log(p_{j_i}^t) + G_{j_i})$ ◁ Fixed noise sampling
  parallel for $j = i$ to $i + L$: ◁ Evaluate
    $p_j^{t+1} \leftarrow p_\theta(\cdot \mid X_{<j}^t)$
  for $j = i$ to $i + L$: ◁ Verify
    $k, X_j^{t+1} \leftarrow$ `MRS`$(p_j^{t+1}, p_j^t, X_j^t)$
    if $k = 0$: **break**
  $i \leftarrow j + 1, t \leftarrow t + 1$
end while
return X

Table 4: Latency breakdown (ms) per NFE step (Janus-Pro 7B, RTX 3090).

Operation	$L=16$	$L=32$	$L=64$
Preprocessing	1.52	1.53	1.58
Transformer Fwd	**26.49**	**27.73**	**36.41**
Logit Proc.	0.16	0.23	0.25
Token Sampling (GS)	0.13	0.13	0.14
Vec. MRS (MC)	1.56	1.58	1.66
Post Processing	0.81	0.82	0.84

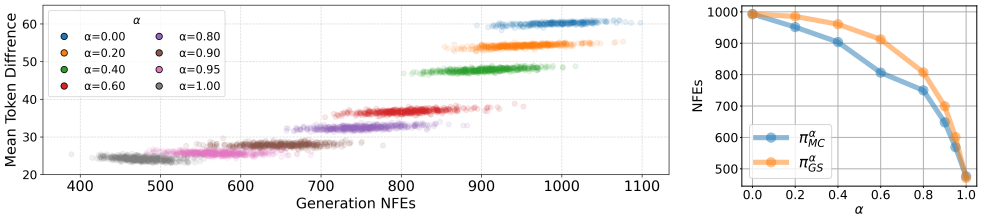

(a) NFEs v.s Token Difference with varying α (π_{MC}, Fig.2 Extended) (b) NFEs v.s α

Figure 5: Coupling Strength Experiments ($L = 32$). Increasing the coupling strength α decrases Mean Token Diffrence and Generatiation NFEs until $\alpha \approx 1$, indicating that pushing collision probability to its theoretical optimal tends to have significant positive effect on minimzing total NFEs.

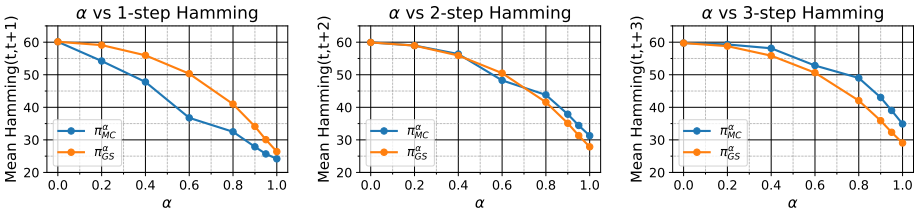

(a) Hamm(t,t+1) (b) Hamm(t,t+2) (c) Hamm(t,t+3)

Figure 6: Multi step behavior of draft tokens when our π_{MC} and π_{GS} applied.

One of the primary advantage of our method is that these *Coupler* introduce almost no overhead compared to standard SJD, in terms of both memory and computation. Please see the actual efficient implementation version of our SCD in Alg. 5,6. In efficient version, π_{MC} can be implemented by simply vectorizing verification loop(Alg. 2, `Line'10`) without *break* and saving the index where the first rejection ($k = 0$) occurs, thereby integrating *drafting and verification into a single operation* to minimize overhead. This can be easily validated by the fact that `Line'5` and `Line'10` in Alg. 2 are strictly identical operations because $p^{(t+1)}$ in `Line'10` becomes $p^(t)$ in next loop's `Line'5`. Similarly, the Gumbel noise in π_{GS} can be efficiently generated online via hashing of the token's global index, and its computation cost is identical to multinomial sampling in π_{SJD}. In Tab. 4, we present a latency breakdown of each component within single NFE step. As shown, *Transformer forward* dominates latency, while overhead of sampling operations, including our couplings, is under 5%. Moreover, since we define $p^{(t)}$ as the final distribution after all logit post-processing(i.e., top-k, CFG), these steps do not affect our exactness guarantee.

B Further Analysis on Behavior of Coupled Sampling

Coupling Strength To more precisely understand what our coupling affects the convergence of SJD, we introduce a notion of *coupling strength* by interpolating between the independent distribution of SJD (π_{SJD}) and our coupling joint distribution (π_{cpl}). We define the α-coupling by,

$$\pi^{\alpha}_{\text{cpl}}(x, y) = \alpha \cdot \pi_{\text{cpl}}(x, y) + (1 - \alpha) \cdot \pi_{\text{ind}}(x, y), \tag{4}$$

Thus $\alpha = 0$ recovers vanilla SJD, and $\alpha = 1$ corresponds to ours. We present validity proof and implementation details of this coupling in in Appendix A.5.

In Fig.5, (a) we plot the mean token difference between consecutive iteration against the resulting NFE by changing α, and (b) summarizes the average NFE on α. We observe a clear monotonic trend: as α increases, both the mean Hamming distance and the NFE consistently decrease, and this improvement continues up to $\alpha \approx 1$. This confirms our hypothesis from Sec.3 that increasing the collision probability in token space directly enhances context stability and, consequently, reduces the total number of function evaluations required for generation.

Multi-Step Behavior While we mainly focused on analyzing and improving theoretically available 1-step behavior of SJD, it is worth to investigate how our coupler affects the longer-step behavior of draft tokens. In Fig. 6, we visualize the Hamming distance (mean token difference) between N-step iterations, $\text{Hamm}(t, t + N)$, when our couplers are applied. As shown, for the 1-step case, π_{MC}

consistently has a smaller distance than π_{GS}, aligning with our theory. However, for multi-step ($N = 2, 3$), this relationship is **reversed** in the high coupling-strength regime. This occurs because, while π_{MC} is optimal for maximizing the 1-step collision probability, there is no non-trivial bound on its multi-step, whereas π_{GS} have a lower bound of $1 - \mathcal{D}_{TV}/(1 + \mathcal{D}_{TV})$ between any pair of multi-step iterations, as shown in Theorem 3. We interpret this as π_{GS} having better *long-range stability* than π_{MC}, and this can be advantageous in tasks where draft prediction is relatively easy, so that keeping early draft tokens unchanged can have more beneficial effect on the final convergence (smaller NFEs) than continually updating them with slightly more accurate information, as is the case in video generation(Tab. 2), which requires only slight modification from given start frame.

C PROOFS

C.1 PROOF OF PROPOSITION 1

Proof. We will first check that $\texttt{MRS}(\cdot)$ returns $Y \sim P$ with input $X \sim Q$. Let the acceptance probability $min(1, p(x)/q(x)) = \alpha(x)$. Then, we can re-write the p.d.f of R.V Y , $y(x)$ as follows

$$y(x) = \alpha(x) \cdot q(x) + (1 - \sum_{x' \in V} \alpha(x') \cdot q(x'))r(x) \tag{5}$$

where $r(x)$ is residual distribution $r(x) = norm(max(0, p(x) - q(x)) = \frac{max(0,p(x)-q(x))}{\sum_{x' \in V} max(0,p(x')-q(x'))}$. We can rewrite the left term as :

$$\alpha(x) \cdot q(x) = min(1, p(x)/q(x)) \cdot q(x) = min(q(x), p(x)) \tag{6}$$

also with the right term :

$$(1 - \sum_{x' \in V} \alpha(x') \cdot q(x'))r(x) = (1 - \sum_{x' \in V} min(q(x'), p(x'))) \frac{max(0, p(x) - q(x))}{\sum_{x' \in V} max(0, p(x') - q(x'))} \tag{7}$$

$$= (1 - \sum_{x' \in V} min(q(x'), p(x'))) \frac{p(x) - min(p(x), q(x))}{\sum_{x' \in V} p(x') - min(p(x'), q(x'))} \tag{8}$$

$$= (1 - \sum_{x' \in V} min(q(x'), p(x'))) \frac{p(x) - min(p(x), q(x))}{1 - \sum_{x' \in V} min(p(x'), q(x'))} \tag{9}$$

$$= p(x) - min(p(x), q(x)). \tag{10}$$

So, adding two terms becomes $p(x)$, the target distribution, as desired.

Now, we will check the acceptance rate :

$$\mathbb{E}_{x' \sim q(x)} \text{min}(1, \frac{p(x')}{q(x')}) = \sum_{x' \in V} q(x') \cdot min(1, \frac{p(x')}{q(x')}) = \sum_{x' \in V} min(p(x'), q(x')) \tag{11}$$

$$= 1/2 \sum_{x' \in V} p(x') + q(x') - |p(x') - q(x')| = 1 - \frac{1}{2} \sum_{x' \in V} |p(x') - q(x')| \tag{12}$$

which is $1 - \mathcal{D}_{TV}(p, q)$.

C.2 PROOF OF PROPOSITION 2

To compute value of C_{SJD}, let $p(x) = p_i^{(t)}(x)$ and $q(x) = p_i^{(t-1)}(x)$ for simplicity.

$$
\begin{aligned}
C_{SJD}(p,q) &\equiv Pr[X^{(t)} = X^{(t-1)}] && (13)\\
&= \sum_{x\in\mathcal{V}} Pr[X^{(t)} = x, X^{(t-1)} = x] && (14)\\
&= \sum_{x\in\mathcal{V}} Pr[X^{(t)} = x] \cdot Pr[X^{(t-1)} = x] \qquad \text{(by independence)} && (15)\\
&= \sum_{x\in\mathcal{V}} p(x)q(x) && (16)
\end{aligned}
$$

Now, we will derive it's upper bound as follows :

$$
\begin{aligned}
(C_{SJD}(p,q))^2 &= \left(\sum_x p(x)q(x)\right)^2 && (17)\\
&\leq \left(\sum_x p(x)^2\right)\left(\sum_x q(x)^2\right) \qquad \text{(by Cauchy-Schwarz)} && (18)
\end{aligned}
$$

Since Renyi-2 entropy is, by definition, $H_2(p) = -\log\left(\sum_x p(x)^2\right) \implies \sum_x p(x)^2 = e^{-H_2(p)}$,

Hence,

$$
\begin{aligned}
(C_{SJD}(p,q))^2 &\leq e^{-H_2(p)} \cdot e^{-H_2(q)} = e^{-(H_2(p)+H_2(q))} && (19)\\
\implies C_{SJD}(p,q) &\leq e^{-\frac{1}{2}(H_2(p)+H_2(q))} && (20)
\end{aligned}
$$

So we can check that independence collision probability is exponentially restricted by their Renyi-2 entropy, regardless of how they are close to each other.

C.3 PROOF OF THEOREM 1

Proof sketch. The theoretical correctness of our approach is based on the marginalization property of the couplings. The standard SJD framework requires that the draft token, which we denote $X_i^{(t)}$, be sampled from the draft distribution $p_i^{(t)}$. If sample $X_i^{(t)}$ follows it's distribution, then correctness of SD framework is guaranteed by Proposition 1. According to **Definition 1**, when we sample a pair $(X_i^{(t)}, X_i^{(t-1)}) \sim \pi(\cdot,\cdot)$ from any valid coupling $\pi \in \Pi_i^{(t)}$, the marginal distribution of the variable $X_i^{(t)}$ is precisely $p_i^{(t)}$. Thus, using the $X_i^{(t)}$ component from the sampled pair is probabilistically identical to sampling a token directly from $p_i^{(t)}$. Since this modification preserves the required sampling distribution for the draft token at each step, the final output distribution of the algorithm is guaranteed to match that of the base model.

C.4 PROOF OF THEOREM 2

We will formally check that $\texttt{MRS}(\cdot)$ satisfies the definition of Coupling. Let the joint distribution of this $\texttt{MRS}(\cdot)$ process $f(x,y)$ is

$$
f(x,y) = q(x)(\alpha(x)\delta_x(y) + (1-\alpha(x))r(y)) \tag{21}
$$

where $\delta_x(y)$ is kronecker-delta symbol.

Let $\alpha(x)$, $r(x)$ is same as we defined on proof of proposition 1. Then for $p(y)$,

$$
\sum_{x\in V} f(x,y) = a(y)\cdot q(y) + (1 - \sum_{x\in V}\alpha(x)q(x))r(y) = p(y) \tag{22}
$$

which directly came out from proof of proposition 1.

Then next, for $q(x)$,

$$\sum_{y \in V} f(x,y) = q(x)\alpha(x) \sum_{y \in V} \delta_x(y) + q(x)(1-\alpha(x)) \sum_{x \in V} r(y) \tag{23}$$

$$= q(x)\alpha(x) + q(x)(1-\alpha(x)) = q(x) \tag{24}$$

So it satisfies the definition of Coupling.

For the coupling cost optimality, it is well studied that any coupling can not have cost greater than $1 - \mathcal{D}_{TV}(P, Q)$ (Lindvall inequality) See (Lindvall, 2002; Bavarian et al., 2016).

C.5 Proof of α-Coupling

For Sec 5.1, we define α-Coupling as follows :

$$\pi^{\alpha}_{\text{cpl}}(x,y) = \alpha \cdot \pi_{\text{cpl}}(x,y) + (1-\alpha) \cdot \pi_{\text{ind}}(x,y), \tag{25}$$

wher $0 \leq \alpha \leq 1$. We will now show this linear-interpolaton of two coupling is still valid coupling.

To check marginal property, we can rewrite it as :

$$\sum_{y \in V} \pi^{a}_{cpl}(x,y) = \sum_{y \in V} [\alpha \cdot \pi_{cpl}(x,y) + (1-\alpha) \cdot \pi_{ind}(x,y)] \tag{26}$$

$$= \alpha \cdot \sum_{y \in V} \pi_{cpl(x,y)} + (1-\alpha) \cdot \sum_{y \in V} \pi_{ind}(x,y) \tag{27}$$

$$= \alpha \cdot p(x) + (1-\alpha) \cdot p(x) = p(x) \tag{28}$$

Same procedure can be applied to $q(y)$.

Implementation To implement linear interpolation of two probability distribution, we can simply sample R.V from Bernoulli distribution, and pick sample with that probability. For example :

Algorithm 7 α-Coupling Implementation

Input: α, Two valid coupling π_a, π_b.
Output: Random Variable X.

```
u ~ U(0,1)
if u ≤ α then
    X, Y ← π_a(x, y)
else
    X, Y ← π_b(x, y)
end if
return X
```

D Related Works

Unified Multimodal Models. Recently, Unified Multimodal Models (Team, 2024; Deng et al., 2025; Hurst et al., 2024), which can process data from multiple modalities such as text, images, and audio for both input and output within a single model, have gained significant attention. The advantage of this paradigm stems from the discovery that models trained on multiple data domains simultaneously exhibit superior performance across a range of tasks compared to single-modality models. This includes enhanced understanding, generation (Chen et al., 2025), complex world reasoning (Hurst et al., 2024), instruction following, and iterative editing (Bai et al., 2023).

Autoregressive Models in Vision Visual generation using an autoregressive (AR) (Team, 2024) approach is a promising method for implementing Unified Multimodal Models. An AR vision model primarily consists of two key components: a Vector Quantizer (Van Den Oord et al., 2017) and a Transformer model (Brown et al., 2020). The vector quantizer divides an image into patches of a specified size and maps each patch to a discrete code from a predefined codebook. This process effectively performs both downsampling and tokenization of the image. Subsequently, similar to autoregressive text generation, a Transformer model is trained to predict these visual token IDs autoregressively. This paradigm enables the learning and inference of diverse data types under a single, unified framework of AR modeling, naturally facilitating stable training, deployment, and capabilities such as in-context learning (Hurst et al., 2024), editing (Liu et al., 2024), and reasoning (Zhao et al., 2025).

Speculative Decoding Speculative Decoding (SD) was first proposed by (Leviathan et al., 2023; Chen et al., 2023) to accelerate the inference speed of Large Language Models (LLMs) without compromising performance by generating multiple tokens at once. Later, (Sun et al., 2023) established a connection between speculative sampling and optimal transport, proving that the token-level acceptance scheme is theoretically optimal for individual tokens. More recently, (Sun et al., 2024b) showed that token-level acceptance is not globally optimal and that the block-wise acceptance approach is the theoretically optimal form of speculative decoding. As the theoretical optimality has been established, the recent research trend in SD has focused on designing better draft models (**?**Brown et al., 2024; Cai et al., 2024) or exploring methods that trade speed for a slight degradation in quality (Bachmann et al., 2025; So et al., 2025).

Parallel Decoding Parallel decoding, or fixed-point iteration $X \leftarrow F(X)$, is a widely used technique for rapidly finding the solution to a specific system, from scientific computing for accelerating the solution of differential equations (Berinde, 2004) to, more recently, fast sampling of diffusion models (Shih et al., 2023). Building on this concept, (Song et al., 2021) first proposed using fixed-point iteration to accelerate the sequential computation of neural networks. Based on the observation that this method guarantees the same result as sequential computation and always at least as faster than sequential when assuming fully parallelization model. Our method can be framed as a novel methodology for accelerating the convergence speed of fixed-point (jacobi) iteration for sequential sampling that operates based on a probabilistic process within a discrete space.

E LIMITATIONS

Since our method relies on parallel computation, the overhead of parallel operations may become significant if the window size or batch size becomes too large, potentially failing to achieve practical speedups, especially in scenarios where the parallel-computation unit is limited. However, this is a structural limitation shared by all Speculative Decoding (SD) methods, and we predict that these limitations will gradually disappear with the advancement of modern hardware.

F EXPERIMENTAL DETAILS

F.1 IMAGE GENERATION

Lumina mGPT: For Lumina-mGPT (Liu et al., 2024) , we use the standard 7B model and experiment with resolution of 768×768. In all experiments, we follow the default settings of vanilla model, temperature $\tau = 1$ and Top-K sampling with $K = 2000$ and guidance scale of $\lambda = 3.0$. We used pytorch 2.3 (Paszke et al., 2019) for the main comparison. For quality evaluation, we generate 5000 images for each MS-COCO 2017 (val) (Lin et al., 2014) prompt and compute FID, IS, CLIP-Score with reference dataset.

Janus Pro : For Janus-Pro (Chen et al., 2025), we use 7B model to generate images at a resolution of 384 × 384. Following the setup of the vanilla Janus-Pro 7B model, 24 × 24 of image tokens are generated with a downsampling size of 16. For sampling, we follws vanilla setting that guidance scale of 5.0 and temperature of 1.0. We also adopted a Top-K logits processor with $K = 1000$. For evaluation, we generate three images for each MS-COCO (val) prompt with different seeds (5000×3) and reported the mean values of the FID, IS, and CLIP score across the seeds.

Table 5: Evaluation results of AR Image generation model, Lumina-mGPT, on Parti-Prompt.

Configuration		NFE (↓)	Latency (↓) (A100)	Acceleration (↑) NFE	Acceleration (↑) Latency	CLIP-Score (↑)
A	*Vanilla AR*	2392	112.29	1.00×	1.00×	32.091
B	SJD (L=16)	1035.3	42.07s	2.31x	2.67x	32.11
D	+ **Ours** (π_{MC})	**817.29**	**32.86s**	**2.92x**	**3.42x**	32.12
D	+ **Ours** (π_{GS})	820.12	32.92s	2.91x	3.41x	32.07
B	SJD (L=32)	1038.2	43.27s	2.30x	2.60x	32.087
D	+ **Ours** (π_{MC})	**647.08**	**26.01s**	**3.69x**	**4.32x**	32.09
D	+ **Ours** (π_{GS})	649.54	26.33s	3.68x	4.26x	32.102
B	SJD (L=64)	1036.2	42.99s	2.31x	2.61x	32.095
D	+ **Ours** (π_{MC})	**548.26**	23.58s	**4.36x**	4.76x	32.113
D	+ **Ours** (π_{GS})	548.75	**23.42s**	**4.36x**	**4.79x**	32.089
C	GSD (G=50)	636.75	25.24s	3.76x	4.45x	32.075

F.2 Video Generation

Cosmos1-autoregressive. We evaluate our method on the *Cosmos-1.0-Autoregressive-4B* video AR model (Agarwal et al., 2025) using a curated subset of 150 clips from the *real-state-10k* dataset (Zhou et al., 2018). For each clip, we provide a 9-frame context to the model and autoregressively generate the next 24 frames, yielding 33-frame sequences in total (9 observed + 24 predicted). Unless otherwise noted, decoding uses nucleus (top-p) sampling with $p = 0.8$ and temperature 1.0.

We compare three decoders: (A) vanilla AR, (B) Speculative Jacobi Decoding (SJD), and (D) our MC-SJD on top of SJD. For SJD-based methods we sweep the parallel verification window $L \in \{16, 32, 64, 128\}$. Speed is reported as (i) **NFE**—the number of sequential target-model evaluations—and (ii) end-to-end wall-clock **Latency** (seconds) measured on a single RTX6000ADA. Quality is measured by **FVD** (lower is better), computed between the generated frames and the corresponding ground-truth future frames of each clip.

G More Visualization

In this section, we provide further details about the visualization settings and discuss our findings based on both quantitative and qualitative results. For image generation, we employed prompts covering diverse categories such as humans, animals, landscapes, close-up shots, fantasy, and paintings. In particular, we included prompts designed to capture physical phenomena such as reflections and waves. We also incorporated descriptors explicitly indicating high-quality imagery (e.g., 8K, sharp focus) to encourage the generation of fine-detailed, realistic images.

As shown in Figs. 7, 8, 9, 10, we observed that our method produced images closely resembling those of the vanilla AR model while achieved more than a 4× reduction in NFE in image generation and 13× in video generation. Moreover, our model was able to generate diverse categories of images, including physical phenomena like reflections and waves, under both the maximal coupling and the Gumbel coupling.

H More Dataset

To validate the generalization capabilities of our methods across various datasets, we conducted a new experiment using the Parti-Prompt (Yu et al., 2022) dataset for text-to-image generation. Specifically, we evaluated generation quality using the CLIP score, and utilized a set of 1,600 distinct real-world text prompts for evaluation; all other experimental settings remain identical to the MS-COCO evaluation described in the main paper.

Config		NFE (↓)	Latency(s)(↓)	CLIP-Score (↑)
A	*Vanilla AR*	576	16.84s	28.98
B	SJD (L=16)	312.00	9.96s	29.02
D	+ **Ours**(π_{MC})	**186.48**	**6.22s**	28.99
D	+ **Ours**(π_{GS})	189.99	6.336	37.13
B	SJD (L=32)	308.17	10.25s	28.97
D	+ **Ours**(π_{MC})	**149.53**	5.471	38.34
D	+ **Ours**(π_{GS})	154.42	**5.388**	37.49

Table 6: Evaluation results of AR Image generation model, Janus-Pro, on Parti-Prompt.

Tables 5 and 6 present the results on the Parti-Prompt dataset. As shown, our methods exhibit acceleration rates of approximately $\sim 4\times$, which are comparable to those observed on the MS-COCO dataset, demonstrating the strong generalization capabilities of our proposed methods.

I USE OF LLM

We used a Large Language Model (LLM) for typo checking, grammar correction, and polishing of our paper draft.

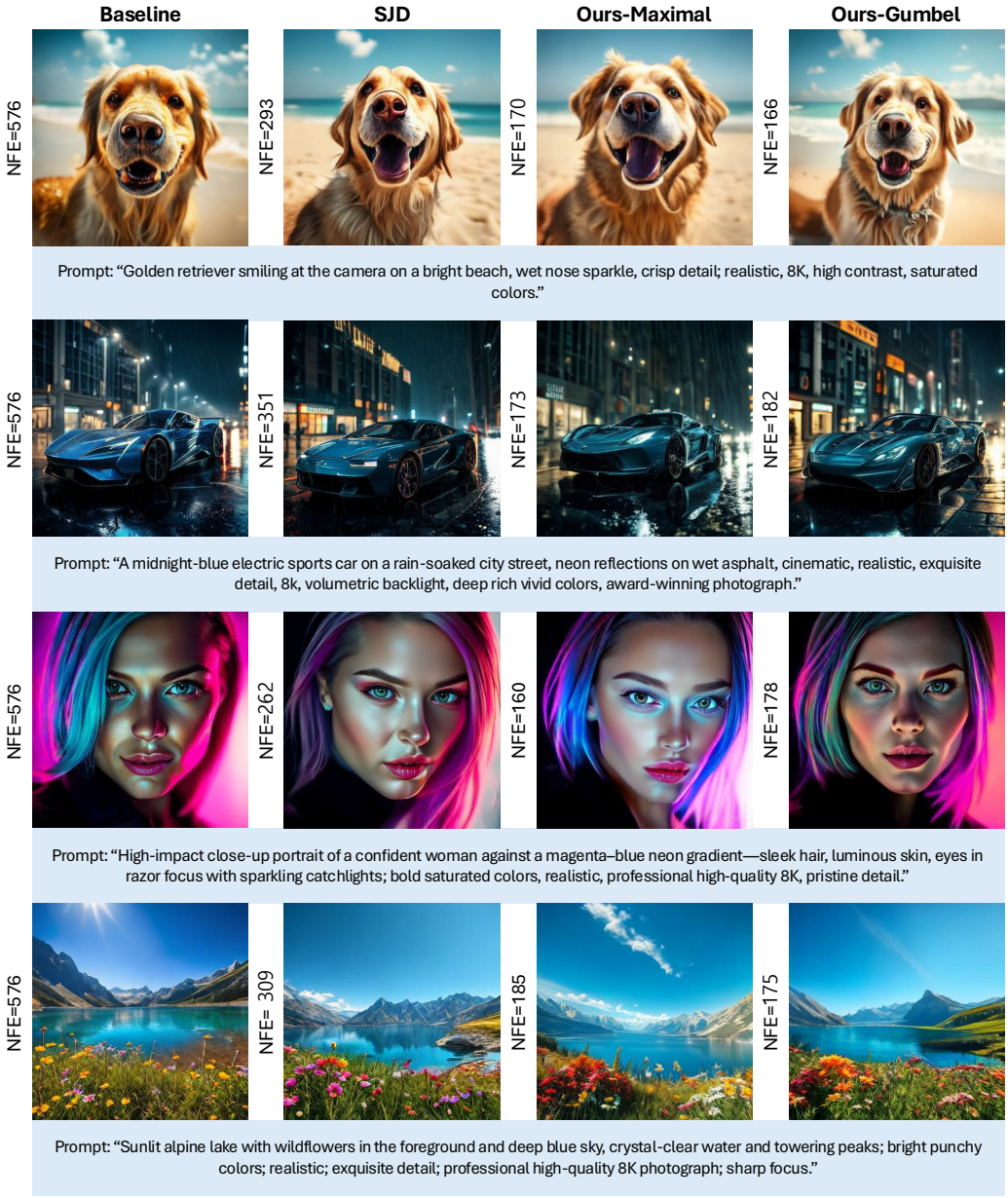

Figure 7: Qualitative comparison on Janus-Pro 7B

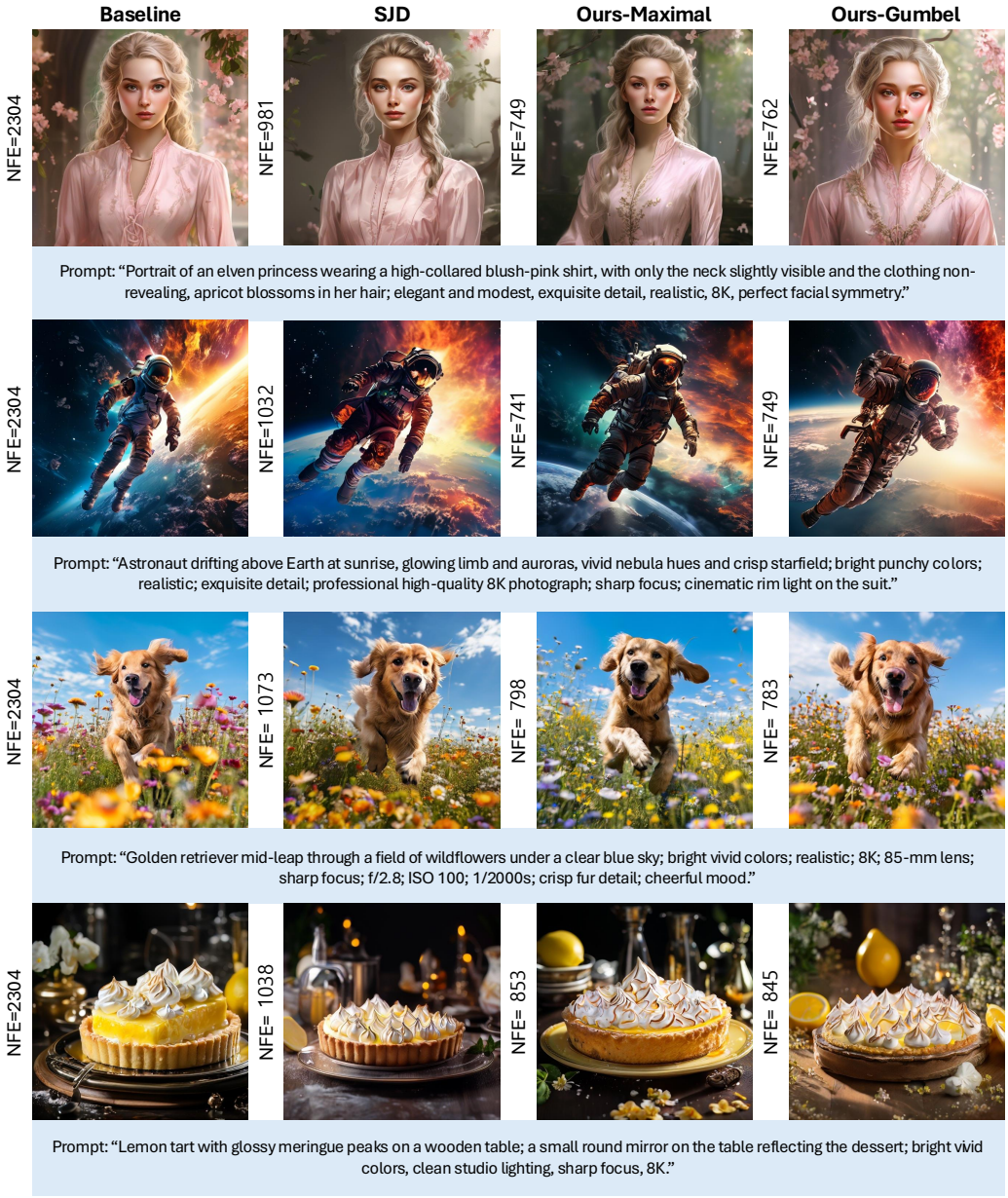

Figure 8: Qualitative comparison on Lumina-mGPT (1.0)

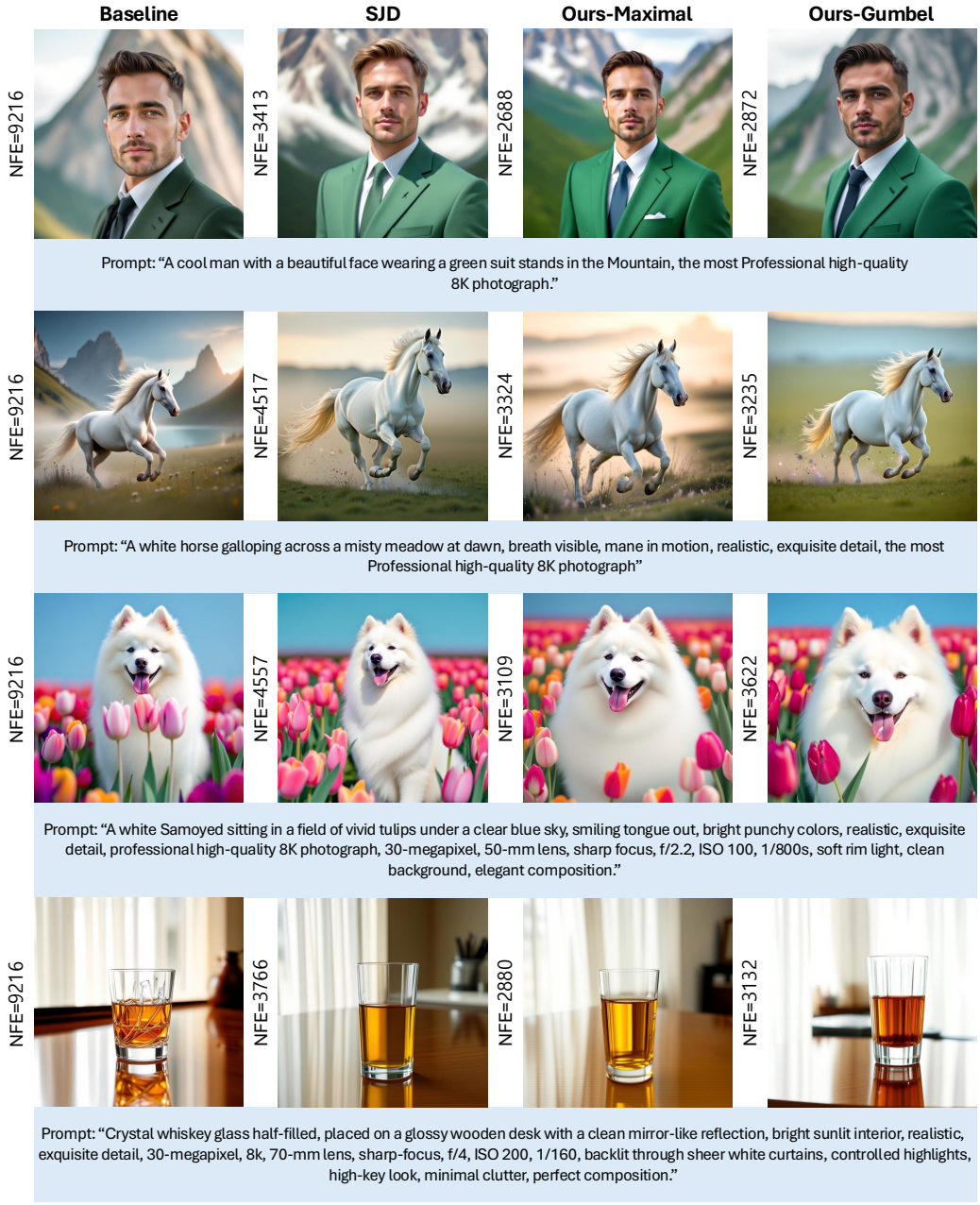

Figure 9: Qualitative comparison on Lumina-mGPT 2.0

Figure 10: Qualitative comparison on Video Generation (Cosmos-1-ar)